CMOS-Compatible Silicon Photonic Sensor for Refractive Index Sensing Using Local Back-Side Release

Patrick Steglich, *Member, IEEE*, Siegfried Bondarenko, Christian Mai, Martin Paul, Michael G. Weller, and Andreas Mai, *Member, IEEE*

***Abstract*— Silicon photonic sensors are promising candidates for lab-on-a-chip solutions with versatile applications and scalable production prospects using complementary metal-oxide semiconductor (CMOS) fabrication methods. However, the widespread use has been hindered because the sensing area adjoins optical and electrical components making packaging and sensor handling challenging. In this work, a local back-side release of the photonic sensor is employed, enabling a separation of the sensing area from the rest of the chip. This approach allows preserving the compatibility of photonic integrated circuits in the front-end of line and metal interconnects in the back-end of line. The sensor is based on a micro-ring resonator and is fabricated on wafer-level using a CMOS technology. We revealed a ring resonator sensitivity for homogeneous sensing of 106 nm/RIU.**

***Index Terms*— Silicon photonic sensor, silicon photonics, integrated photonics, refractive index sensing, photonic biosensor.**

I. Introduction

SILICON-based photonic biosensors integrated into a semiconductor chip technology can lead to significant advances in point-of-care applications, food diagnostics, and environmental monitoring through the rapid and precise analysis of various substances [1]. In recent years, there has been an increasing interest in sensors based on photonic integrated circuits (PIC) because they give rise to cost-effective, scalable and reliable on-chip biosensors for a broad market. The PIC technology employs typically silicon-on-insulator (SOI) wafer, which is the most attractive approach from a commercial point of view since it provides a scalable platform for mass production using complementary metal-oxide semiconductor (CMOS) fabrication processes [2].

Manuscript received July 30, 2020; revised August 18, 2020; accepted August 21, 2020. Date of publication August 24, 2020; date of current version September 3, 2020. This work was supported in part by the ATTRACT Project funded by European Council (EC) under Grant 777222 and in part by the European Regional Development Fund under Grant 10.13039/501100008530. *(Corresponding author: Patrick Steglich.)*

Patrick Steglich and Andreas Mai are with the IHP—Leibniz-Institut für innovative Mikroelektronik, 15236 Frankfurt (Oder), Germany, and also with the Department of Photonics, Technische Hochschule Wildau, 15745 Wildau, Germany (e-mail: patrick.steglich@th-wildau.de).

Siegfried Bondarenko is with the Department of Photonics, Technische Hochschule Wildau, 15745 Wildau, Germany.

Christian Mai is with the IHP—Leibniz-Institut für innovative Mikroelektronik, 15236 Frankfurt (Oder), Germany.

Martin Paul and Michael G. Weller are with the Federal Institute for Materials Research and Testing (BAM), 12489 Berlin, Germany.

Color versions of one or more of the figures in this letter are available online at http://ieeexplore.ieee.org.

Digital Object Identifier 10.1109/LPT.2020.3019114

Once the photonic chip is fabricated, it can be used for homogeneous sensing of refractive index variations or it is employed for surface sensing by coating the silicon waveguide with a covalently attached sensing layer. The sensing layer determines the specific detection and, hence, the application. This step, however, is independent of the fabrication of the chip, making the PIC technology based on SOI wafer attractive for both, science and industry. A further advantage of PIC-based biosensors is the possibility to realize sensor arrays using, e.g., an inkjet surface functionalization process [3]. This allows for the detection of several substances in parallel (multiplexing) [4]. During the last two decades, integrated photonic sensors have been intensively studied in terms of sensitivity and reliability [5].

However, the bottle-neck for a transfer from laboratory to industry is the position of the sensing area, since it adjoins optical and electronic components. This prohibits cost-effective packaging and makes the sensor handling impractical. Current photonic sensors based on PIC technologies are interacting with the analyte from the top side of the photonic chip; i.e., the sensor element such as a ring resonator is released by etching through the oxide cladding on top of the SOI waveguide. Here, the light source, sensor and light detector are on the same side of the chip. The most severe problems are the packaging and handling because PIC-based chips are always millimeter-sized, obstructing the integration of electrical interconnects and microfluidics for high-throughput.

Currently, these problems are tackled by enlarging the chip size or by using sophisticated microfluidics [6] or packaging techniques [7]. This dramatically increases costs and prohibits ease of use for the surface functionalization [8]. Further, the front-side release makes a monolithic integration of silicon photonic sensors into a CMOS or SiGe BiCMOS technology challenging due to the complex material stack of the back-end of line (see Figure 1). In general, silicon photonic sensors need to be sealed, connected to pumping peripherals, and often bear electrical and optical connections [9].

To tackle this general problem, we developed a novel integration approach to separate the sensing area from the rest of the chip by releasing the silicon photonic sensor from the back-side of the chip. For the first time, this gives perspective to a fully packaged, cost-effective photonic sensor platform that can be monolithically integrated. As proof-of-principle, this work aims to demonstrate homogeneous sensing of NaCl at various concentrations in DI water.

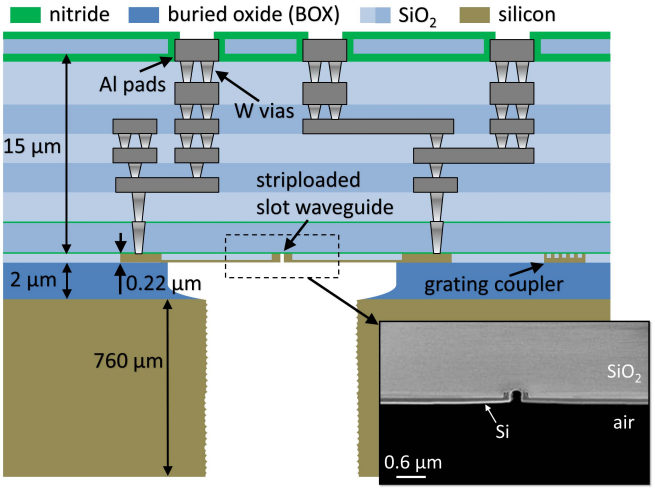

Fig. 1. Schematic cross-section of a back-side released silicon slot waveguide with complete back end of line. A local back-side release is used to realize a trench ranging from the silicon substrate to the silicon device layer. The inset shows a scanning electron microscope image of a fabricated device.

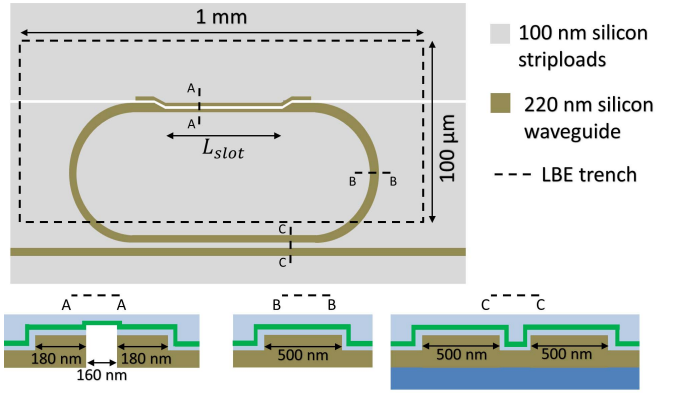

Fig. 2. Schematic top view of the ring resonator with cross-sections of different waveguides. The local back-side etched (LBE) trench has an area of 1000 μm $\times$ 100 μm.

II. Sensor Integration Concept and Fabrication

The photonic chip is fabricated in a PIC technology using 200 mm SOI wafer with a 220 nm thick c-Si on top of a 2 μm buried oxide, as shown in Figure 1. The idea is to shift the sensor from the crowded and water-sensitive front-side of the chip to the back-side. This is realized by a local back-side release, following the work in [10]. In this case, the photonic sensor is released from the wafer back-side by a dry etch followed by a wet etch to locally remove the silicon substrate and the buried oxide, respectively. To protect the back-end of line against the relatively long etching time and to enable a back-side integration on wafer-level, the passivation of the top metal pads is modified following the procedure reported in [11]. It is worth to mention that the lowest grating coupler loss of 4 dB was achieved with the fabrication flow using a standard passivation module, while a 5 dB grating coupler loss was observed with the adjusted passivation module. For the local back-side etch (LBE), a planarization of the back-side and the deposition of SiO_2 as hard mask is required. The hard mask is patterned with DUV lithography and reactive ion etching, while deep reactive ion etching process is employed to etch the 760 μm silicon substrate.

To test the viability of the fabricated photonic sensor, we perform homogeneous sensing experiment to evaluate the sensitivity. The ring resonator sensitivity for homogeneous sensing is defined as

$$S_{RR} = \frac{\Delta\lambda_{res}}{\Delta n_f}, \tag{1}$$

where $\Delta\lambda_{res}$ refers to the resonance wavelength shift and Δn_f to the refractive index change of the fluid. Developing application-specific sensors is typically a balancing act between sensitivity and optical losses traded off against each other within the limitations of the present fabrication flow. On the one hand, narrowing the line width ($FWHM$) reduces the detection limit. This can be achieved by lowering optical losses within the ring resonator. On the other hand, lower losses are primary observed through strong confinement inside the silicon waveguide, which leads to a lower interaction with the fluid. As a consequence, the ring resonator sensitivity is reduced at the same time. One strategy to find a trade-off is the use of a partially slotted ring resonator [12]. This approach combines a rib waveguide with a slot waveguide. The slot waveguide exhibits higher optical losses, which are caused by random line-edge sidewall roughness scattering. However, its high sensitivity makes it suitable for sensing applications [13]. Here, we use a rib waveguide and a strip-loaded slot waveguide, as shown in Figure 2. The ring resonator is located in the middle of the LBE area. A racetrack configuration is used to introduce the slot waveguide within the straight part of the ring. The silicon strip loads are necessary to avoid an over etch of the silicon waveguide and are used as etch stop. The rib waveguide has a width of 500 nm and the slot waveguide has a rail width of 180 nm and a slot width of 160 nm. Figure 3 shows the optical field distribution of a back-side released slot and rib waveguide having the employed waveguide geometries. At a wavelength of 1550 nm, we have estimated a field confinement factor inside the fluid region of $\Gamma_{rib}^{fluid} = 0.1$ and $\Gamma_{slot}^{fluid} = 0.22$ for the rib and slot waveguide, respectively. Figure 3 plots the relative effective refractive index over the refractive index of fluid. The relative effective refractive index is defined as $\Delta n_{eff} = n_{eff}(C) - n_{eff}(0wt\%)$, where C represents the concentration of NaCl in DI water. The waveguide sensitivity can be deduced from the slope of the linear fitting function. It is revealed that the slot waveguide with thinner strip loads (50 nm) exhibits the highest waveguide sensitivity of $S_{WG} = 0.323$, while the rib waveguide shows no significant dependence of the waveguide sensitivity on the strip load height. However, due to fabrication limitations, we used strip loads with a thickness of 100 nm.

III. Results

Figure 4 shows the observed optical spectrum of the back-side released micro-ring resonator, measured with a tunable laser having a wavelength resolution of 5 pm. We inferred an extinction ratio of $ER = 20$ dB and a full width at half

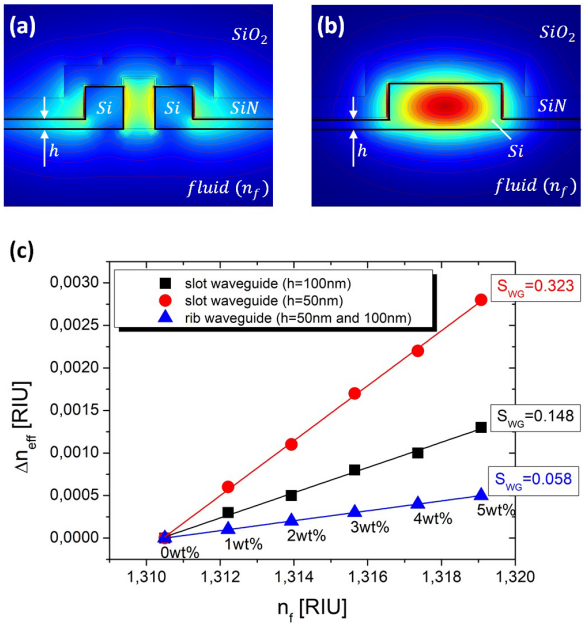

Fig. 3. Optical field distributions in a slot (a) and rib waveguide (b) at wavelength of 1550 nm. Relative effective refractive index as a function of the refractive index of the fluid is shown in (c). NaCl in DI water was considered as fluid having different concentrations, as indicated in the graph.

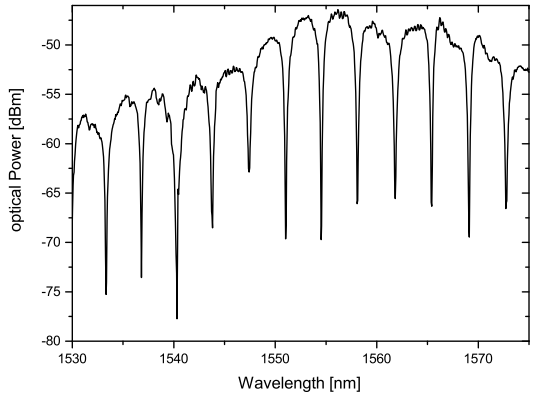

Fig. 4. Optical spectrum of the back-side released micro-ring resonator.

maximum of $FWHM = 0.55$ nm ($Q = \lambda/FWHM \approx 2800$) from this figure. The sample is fixed on a hot plate in this experiment, and by tuning the temperature, we have revealed a temperature sensitivity of $S_T = 92$ pm/K, which is comparable with a similar ring resonator that has been opened from the top [14]. The experimental results of this experiment are shown in Figure 5.

As proof of principle, we have performed homogeneous sensing experiments with different concentrations of NaCl in DI water. For this experiment, we employed a super luminescence diode and an optical spectrum analyzer with a wavelength resolution of 30 pm, while the photonic chip is fixed on a 3D-printed sample holder with a fluid reservoir. The grating coupler is TE-polarization selective and were used in order to couple the light from a single-mode fiber into the chip. TE-mode operation is achieved by maximizing the output signal through a paddle-style fiber polarization

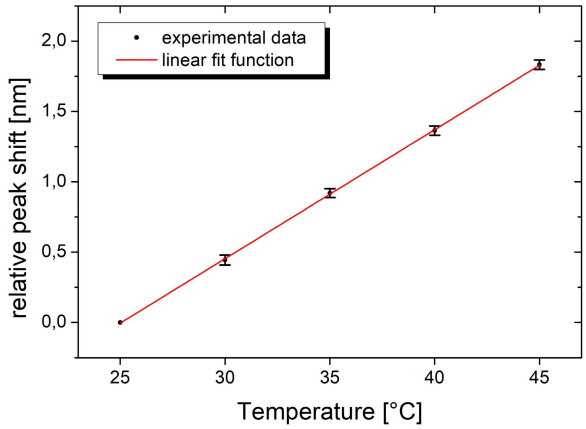

Fig. 5. Relative peak shift as function of the temperature. The slope of the linear fit function equates the temperature sensetivity.

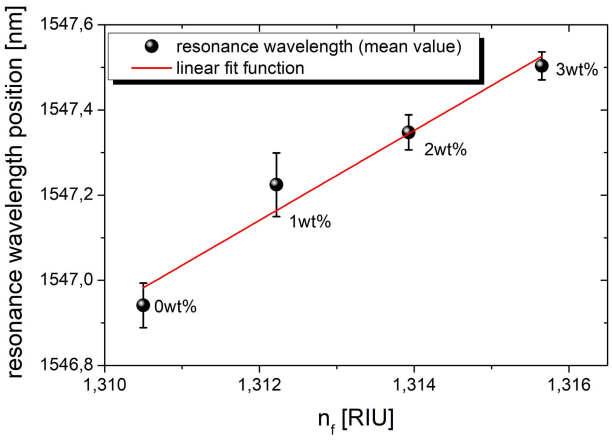

Fig. 6. Resonance wavelength shift as function of the refractive index of the fluid. The concentration of NaCl in DI water is indicated at each measurement point. The slope of the linear fit gives the ring resonator sensitivity.

controller. Liquids with a different weight percentage of NaCl ranging from $0wt\%$ to $3wt\%$ were dropped onto the silicon photonic sensor using a pipette. The refractive index n_f of the NaCl solved in DI water at different concentrations $C(wt\%)$ and at a wavelength of 1550 nm can be calculated by $n_f(wt\%) = 1.3105 + 0.17151 \times C(wt\%)/100$ [15], [16]. For the selected concentrations from $0wt\%$ to $3wt\%$ the refractive index of the solution hence ranges from 1.3105 to 1.3157. We used the same ring resonator for all measurements. After each measurement, the chip was carefully cleaned and dried. To characterize the homogeneous sensing, we plotted the resonance wavelength as a function of the refractive index of the fluid (NaCl in DI water) in Figure 6. Through a linear regression, we have deduced a ring resonator sensitivity of $S_{RR} = 106$ nm/RIU, which is comparable with values reported for similar micro-ring resonators released from the front-side [12].

IV. Discussion

The presented results in terms of thermal sensitivity and homogeneous sensing demonstrate that the back-side released

sensor shows similar performance as a sensor that is released from the top, confirming the viability of the proposed sensor integration concept. The current ring resonator sensitivity can be further increased by using an optimized waveguide structure. The present slot waveguide was optimized for a strip load height of 50 nm (see Figure 3). However, we used a strip load height of 100 nm since the local back-side etch has partly damaged the 50 nm strip loads due to cracks induced by stress. Besides that, advanced waveguide structures such as subwavelength grating waveguides give perspective to further increase the sensitivity [17]. For example, Luan et al. have demonstrated a sub-wavelength multibox waveguide microring resonator with a homogeneous sensitivity of 579.5 nm/RIU [18].

However, the proposed local back-side release photonic sensor platform opens a new route towards high-throughput packaging because the optical and electrical interconnects are on the same side of the chip, while the fluidic can be easily introduced from the opposite side. Moreover, it allows a monolithic integration of photonic sensors, optoelectronic as well as electronic components on the same chip because the back-end of line is completely accessible.

V. Conclusion

For the first time, we have presented an approach to fully integrate silicon photonic sensors in a PIC technology, having a complete back-end of line. A local back-side etch process is employed to release the photonic sensor from the back-side of a 200 mm SOI wafer. As proof of principle, refractive index sensing (homogeneous sensing) was demonstrated using a partially slotted ring resonator. A ring resonator sensitivity of $S_{RR} = 106$ nm/RIU is revealed, which is similar to values observed with front-side released sensors having a comparable resonator geometry. The CMOS-compatibility and the possibility to use the complete back-end of line to connect photonic sensor elements with electronic devices on the same chip as well as the separation of the photonic sensor from optical and electrical connections make the back-side integration concept attractive for future sensor systems.

References

[1] E. Luan, H. Shoman, D. Ratner, K. Cheung, and L. Chrostowski, "Silicon photonic biosensors using label-free detection," *Sensors*, vol. 18, no. 10, p. 3519, Oct. 2018. [Online]. Available: https://www.mdpi.com/1424-8220/18/10/3519

[2] A. Rahim *et al.*, "Open-access silicon photonics platforms in Europe," *IEEE J. Sel. Topics Quantum Electron.*, vol. 25, no. 5, pp. 1–18, Sep. 2019.

[3] J. T. Kirk, G. E. Fridley, J. W. Chamberlain, E. D. Christensen, M. Hochberg, and D. M. Ratner, "Multiplexed inkjet functionalization of silicon photonic biosensors," *Lab Chip*, vol. 11, no. 7, pp. 1372–1377, 2011, doi: 10.1039/C0LC00313A.

[4] R. M. Graybill, M. C. Cardenosa-Rubio, H. Yang, M. D. Johnson, and R. C. Bailey, "Multiplexed microRNA expression profiling by combined asymmetric PCR and label-free detection using silicon photonic sensor arrays," *Anal. Methods*, vol. 10, no. 14, pp. 1618–1623, 2018.

[5] J. Milvich, D. Kohler, W. Freude, and C. Koos, "Surface sensing with integrated optical waveguides: A design guideline," *Opt. Express*, vol. 26, no. 16, pp. 19885–19906, Aug. 2018. [Online]. Available: http://www.opticsexpress.org/abstract.cfm?URI=oe-26-16-19885

[6] Z. Liao *et al.*, "Microfluidic chip coupled with optical biosensors for simultaneous detection of multiple analytes: A review," *Biosensors Bioelectron.*, vol. 126, pp. 697–706, Feb. 2019. [Online]. Available: http://www.sciencedirect.com/science/article/pii/S095656631830928X

[7] L. Laplatine, E. Luan, K. Cheung, D. M. Ratner, Y. Dattner, and L. Chrostowski, "System-level integration of active silicon photonic biosensors using fan-out wafer-level-packaging for low cost and multiplexed point-of-care diagnostic testing," *Sens. Actuators B, Chem.*, vol. 273, pp. 1610–1617, Nov. 2018. [Online]. Available: http://www.sciencedirect.com/science/article/pii/S0925400518312620

[8] J. Wang, M. M. Sanchez, Y. Yin, R. Herzer, L. Ma, and O. G. Schmidt, "Silicon-based integrated label-free optofluidic biosensors: Latest advances and roadmap," *Adv. Mater. Technol.*, vol. 5, no. 6, Jun. 2020, Art. no. 1901138, doi: 10.1002/admt.201901138.

[9] Y. Temiz, R. D. Lovchik, G. V. Kaigala, and E. Delamarche, "Lab-on-a-chip devices: How to close and plug the lab?" *Microelectron. Eng.*, vol. 132, pp. 156–175, Jan. 2015. [Online]. Available: http://www.sciencedirect.com/science/article/pii/S0167931714004456

[10] C. Mai, P. Steglich, M. Fraschke, and A. Mai, "Back side release of slot waveguides for integration of functional materials in a silicon photonic technology with full BEOL," *IEEE Trans. Compon., Packag., Manuf. Technol.*, early access, Jul. 22, 2020, doi: 10.1109/TCPMT.2020.3011149.

[11] C. Mai, P. Steglich, and A. Mai, "Adjustment of the BEOL for back side module integration on wafer level in a silicon photonic technology," in *Proc. MikroSystemTechnik; Congr.*, Oct. 2019, pp. 1–4.

[12] P. Steglich *et al.*, "Hybrid-waveguide ring resonator for biochemical sensing," *IEEE Sensors J.*, vol. 17, no. 15, pp. 4781–4790, Aug. 2017.

[13] D. M. Kita, J. Michon, S. G. Johnson, and J. Hu, "Are slot and subwavelength grating waveguides better than strip waveguides for sensing?" *Optica*, vol. 5, no. 9, pp. 1046–1054, 2018. [Online]. Available: http://www.osapublishing.org/optica/abstract.cfm?URI=optica-5-9-1046

[14] A. Mai, S. Bondarenko, C. Mai, and P. Steglich, "Photonic thermal sensor integration towards electronic-photonic-IC technologies," in *Proc. ESSDERC-49th Eur. Solid-State Device Res. Conf. (ESSDERC)*, Sep. 2019, pp. 254–257.

[15] H. Su and X. G. Huang, "Fresnel-reflection-based fiber sensor for on-line measurement of solute concentration in solutions," *Sens. Actuators B, Chem.*, vol. 126, no. 2, pp. 579–582, Oct. 2007.

[16] X. Tu *et al.*, "Thermal independent silicon-nitride slot waveguide biosensor with high sensitivity," *Opt. Express*, vol. 20, no. 3, pp. 2640–2648, 2012. [Online]. Available: http://www.opticsexpress.org/abstract.cfm?URI=oe-20-3-2640

[17] X. Xu, Z. Pan, C.-J. Chung, C.-W. Chang, H. Yan, and R. T. Chen, "Subwavelength grating metamaterial racetrack resonator for sensing and modulation," *IEEE J. Sel. Topics Quantum Electron.*, vol. 25, no. 3, pp. 1–8, May 2019.

[18] E. Luan *et al.*, "Enhanced sensitivity of subwavelength multibox waveguide microring resonator label-free biosensors," *IEEE J. Sel. Topics Quantum Electron.*, vol. 25, no. 3, pp. 1–11, May 2019.